Luminescence Spectroscopy and Emitting-State Properties of $Pd(SCN)_4^{2-}$ in Crystals

Yanick Pelletier and Christian Reber*

Département de Chimie, Université de Montréal, Montréal QC H3C 3J7, Canada

Received February 8, 2000

Luminescence from $K_2Pd(SCN)_4$, $[K(18\text{-crown-6})]_2Pd(SCN)_4$, and (2-diethylammonium *N*-(2,6-dimethylphenyl)-acetamide)$_2Pd(SCN)_4$ is observed between 10000 and 14500 cm^{-1} (1000 and 690 nm) at temperatures below 100 K. Luminescence lifetimes of up to 4.15 ms are measured at 10 K. The spectra show resolved vibronic progressions with average energy intervals of 278 and 150 cm^{-1}. The average Stokes shift determined from the luminescence and excitation spectra is 4100 cm^{-1}. Average dimensionless emitting-state distortions Δ of 3.75 and 1.7, corresponding to Huang−Rhys parameters *S* of 7.0 and 1.5, along the two modes are obtained from calculated luminescence spectra.

Introduction

Square-planar complexes of platinum(II) and palladium(II) with d^8 electron configuration and D_{4h} point group symmetry are ideal systems to study vibronic effects involving low-energy excited states. These compounds often luminesce and show well-defined absorption bands.[1−14] In the following, we present excitation and luminescence spectra to characterize the lowest-energy excited electronic state of $Pd(SCN)_4^{2-}$. We use symmetry labels for the idealized D_{4h} point group and choose the *z* axis of the Cartesian coordinate system parallel to the 4-fold axis in order to be consistent with the literature on square-planar transition metal complexes.

The electron configuration of the $^1A_{1g}$ ground state of square-planar d^8 complexes is $a_{1g}(d_{z^2})^2b_{2g}(d_{xy})^2e_g(d_{xz},d_{yz})^4b_{1g}(d_{x^2-y^2})^0$. These orbital energy levels lead to two distinct classes of excited states: first the orbitally nondegenerate states arising from electron configurations with singly occupied nondegenerate orbitals and second the degenerate $^{1,3}E_g$ excited states arising from electron configurations with an incomplete occupation of the e_g (d_{xz},d_{yz}) levels. All electronic transitions involve the population of the σ antibonding b_{1g} orbital, and we therefore expect an elongation of all metal−ligand bonds in the excited crystal field states, corresponding to an offset of their potential surface minima along the normal coordinate of the totally symmetric (a_{1g}) stretching mode. In addition, the $^{1,3}E_g$ excited states have been shown to undergo distortions corresponding to an elongation of one pair of opposite metal−ligand bonds and to a bond length decrease for the other pair of bonds, leading to an offset of the excited-state potential minima along the b_{1g} normal coordinate. The second possible distortion of the $^{1,3}E_g$ excited states involves the b_{2g} ligand−metal−ligand bending mode, a distortion that has to our knowledge not been observed in the electronic spectra of high-symmetry square-planar complexes. The vibronic structure observed in luminescence, excitation, and absorption spectra can be used to experimentally distinguish between orbitally degenerate and nondegenerate emitting states and to determine the importance of the distortions that can occur along the a_{1g}, b_{1g}, and b_{2g} modes in the $^{1,3}E_g$ excited states.

The lowest-energy absorption bands of square-planar complexes are often very weak and were overlooked in the literature even for well-studied halide complexes.[9,15] A number of exactly square-planar complexes such as $PtCl_4^{2-}$, $PdCl_4^{2-}$, and $PdBr_4^{2-}$ have been thoroughly characterized by luminescence spectroscopy, the most powerful technique to probe the lowest-energy excited state.[10,11,14,16] K_2PtCl_4 shows a single resolved progression with a spacing determined by a missing-mode effect (MIME[17]) involving the a_{1g} and b_{1g} stretching modes.[11] The spectrum of K_2PdBr_4 is dominated by a progression in the a_{1g} mode with shoulders corresponding to the b_{1g} vibration.[14] The excited-state distortions for $PdBr_4^{2-}$ determined from luminescence spectra[14] were reproduced by density functional calculations,[18] indicating that the emitting-state structure is predominantly determined by the molecular electronic structure and only to a lesser extent by packing effects of the complexes in a crystal. Lower-symmetry complexes with palladium−sulfur bonds, such as Pd(maleonitriledithiolate)$_2^{2-}$, show resolved vibronic structure that involves many vibrational modes.[12] To our knowledge, $Pd(SCN)_4^{2-}$ represents the first square-planar complex for which a resolved luminescence spectrum with vibronic structure involving the stretching *and* bending modes expected for the $^1A_{1g} \leftrightarrow {}^3E_g$ excitation is reported and analyzed.

* Author for correspondence.

(1) Martin, D. S.; Tucker, M. A.; Kassman, A. J. *Inorg. Chem.* **1965**, *4*, 1682.
(2) Martin, D. S.; Tucker, M. A.; Kassman, A. J. *Inorg. Chem.* **1966**, *5*, 1298.
(3) Martin, D. S. *Inorg. Chim. Acta, Rev.* **1971**, *5*, 107.
(4) Martin, D. S.; Bonte, J. L.; Rush, R. M.; Jacobson, R. A. *Acta Crystallogr.* **1975**, *B31*, 2538.
(5) Patterson, H. H.; Godfrey, J. J.; Kahn, S. M. *Inorg. Chem.* **1972**, *11*, 2872.
(6) Gliemann, G.; Yersin, H. *Struct. Bonding* **1985**, *62*, 87.
(7) Francke, E.; Moncuit, C. *Theor. Chim. Acta* **1973**, *29*, 319.
(8) Francke, E.; Moncuit, C. *C. R. Séances Acad. Sci., Sér. B* **1970**, *271*, 741.
(9) Tuszynski, W.; Gliemann, G. *Z. Naturforsch.* **1979**, *34a*, 211.
(10) Yersin, H.; Otto, H.; Zink, J. I.; Gliemann, G. *J. Am. Chem. Soc.* **1980**, *102*, 951.
(11) Preston, D. M.; Güntner, W.; Lechner, A.; Gliemann, G.; Zink, J. I. *J. Am. Chem. Soc.* **1988**, *110*, 5628.
(12) Güntner, W.; Gliemann, G.; Kunkely, H.; Reber, C.; Zink, J. I. *Inorg. Chem.* **1990**, *29*, 5238.
(13) Reber, C.; Zink, J. I. *J. Phys. Chem.* **1991**, *95*, 9151.
(14) Pelletier, Y.; Reber, C. *Inorg. Chem.* **1997**, *36*, 721.
(15) Vanquickenborne, L. G.; Ceulemans, A. *Inorg. Chem.* **1981**, *20*, 796.
(16) Reber, C.; Zink, J. I. *Comments Inorg. Chem.* **1992**, *13*, 177.
(17) Tutt, L.; Zink, J. I. *J. Am. Chem. Soc.* **1986**, *108*, 5830.
(18) Harvey, P. D.; Reber, C. *Can. J. Chem.* **1999**, *77*, 16.

10.1021/ic000133l CCC: $19.00
Published on Web 09/08/2000

Table 1. Summary of Spectroscopic Results

parameter	$[K(18\text{-crown-}6)]_2[Pd(SCN)_4]$	$K_2Pd(SCN)_4$	$(LC)_2Pd(SCN)_4$
luminescence max E_{max} (cm^{-1})	12810	12540	12780
luminescence origin (cm^{-1})[a]			14450
luminescence lifetime at E_{max} (μs)	710 (10 K)	4150 (7 K)	514 (10 K)
	87 (100 K)	850 (20 K)	257 (30 K)
main progression interval (cm^{-1})		250 ± 100	276 ± 8
excitation max (cm^{-1})	17000	16690	16860
Stokes shift (cm^{-1})	4190	4120	4080
Raman freq (cm^{-1})[b]	281[c]	117 (b_{2g})	132 (b_{2g}, strong)
	181[c]	137 (b_{2g}, strong)	152 (b_{2g})
		166 (b_{2g}, strong)	167 (b_{2g})
		260 (b_{1g})	260 (b_{1g})
		277 (a_{1g}, strong)	278 (a_{1g}, strong)
			293

[a] Highest-energy maximum of the 10 K luminescence spectrum. [b] Measured at 83 K, only transitions between 100 and 300 cm^{-1} are given. [c] Measured at 300 K.

We present new luminescence and low-energy excitation spectra of $Pd(SCN)_4^{2-}$ in three different crystalline environments, $K_2Pd(SCN)_4$, $[K(18\text{-crown-}6)]_2Pd(SCN)_4$, and (2-diethylammonium *N*-(2,6-dimethylphenyl)acetamide)$_2Pd(SCN)_4$, and we analyze the vibronic structure of the luminescence spectra, their intensities, and lifetimes as a function of temperature. The spectroscopic results are compared to the HOMO and LUMO orbitals obtained from density functional calculations to qualitatively illustrate the importance of the bending modes in the vibronic structure of the luminescence spectra.

Experimental Section

$K_2Pd(SCN)_4$ was prepared from an aqueous solution of K_2PdCl_4 (Strem Chemicals) by adding KSCN to the solution and refluxing for 2 h.[19,20] The product was recrystallized from 1-butanol, and crystals were obtained as dark red needles. An excess of the crown ether 18-crown-6 was added to the butanol solution, and pale red crystals of $[K(18\text{-crown-}6)]_2Pd(SCN)_4$ were obtained in the refrigerator. (2-Diethylammonium *N*−(2,6-dimethylphenyl)acetamide)$_2Pd(SCN)_4$ was obtained from an aqueous solution of $Pd(SCN)_4^{2-}$ to which 2-diethylammonium *N*-(2,6-dimethylphenyl)acetamide hydrochloride (lidocaine hydrochloride) was added.[21] We abbreviate this ammonium cation as LC throughout the following. The compound was recrystallized from ethanol, and all materials were analyzed by IR,[22] Raman, excitation, and luminescence spectroscopy.

The spectroscopic instrumentation for steady-state and time-resolved luminescence has been described before.[23] Luminescence spectra were measured with a Xe lamp filtered through a copper sulfate solution and Schott BG18 filters. The samples were cooled in a helium gas-flow cryostat (Oxford Instruments CF 1204). The emitted light was filtered by a RG 610 filter, dispersed through a 0.75 m monochromator (Spex 1800 II) and detected with photomultipliers (Hamamatsu R4632, R928 or R406). All luminescence spectra were corrected for detector response by calibration with a reference tungsten lamp (Oriel 63350).[23] An additional 0.5 m monochromator (Spex 500M) was used to scan the excitation wavelength. For all excitation spectra, a KV 418 filter was used in front of the excitation monochromator and a RG 780 filter in front of the emission monochromator.

Luminescence lifetimes were measured with the 308 nm line of a XeCl excimer laser (Lumonics Hyperex 420 SMB, 20 ns pulse width). The laser power did not exceed 5 mJ/pulse measured at the exit window of the laser. The time-dependent luminescence signal was dispersed by the 0.5 m monochromator and detected by a cooled Hamamatsu R928 photomultiplier and a digital oscilloscope (Tektronix TDS 380) triggered by a Si photodiode (Thorlabs FDS 100) detecting the excitation pulse.

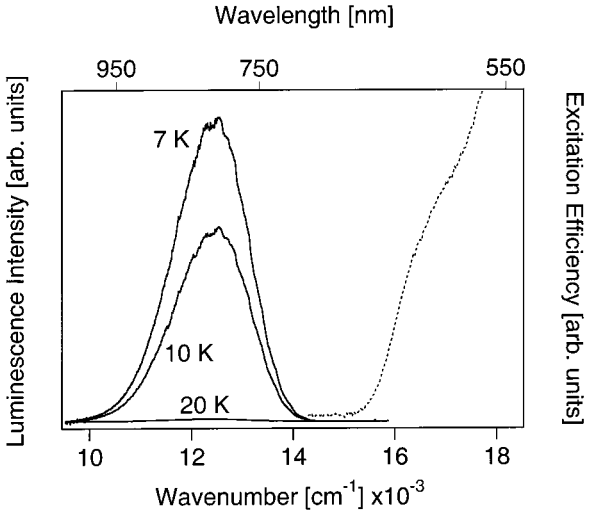

Figure 1. Luminescence and excitation spectra of $K_2Pd(SCN)_4$. Luminescence spectra at 7, 10, and 20 K (top to bottom) are given as solid lines; the excitation spectrum at 7 K is shown as a dotted line.

Raman spectra were measured with a Renishaw System 3000 spectrometer using the 514.5 nm line of an Ar^+ ion laser as excitation source. This choice of excitation wavelength leads to resonance enhancements of the metal−ligand vibrations that determine the vibronic structure of the luminescence spectra.[9]

Spectroscopic Results

The experimental quantities determined from luminescence, excitation, and Raman spectra are summarized in Table 1. Luminescence spectra of $Pd(SCN)_4^{2-}$ in the three different crystalline environments are presented in Figures 1−3 . A broad luminescence band between 10000 and 14000 cm^{-1} is observed for all compounds. The 7 K spectrum of $K_2Pd(SCN)_4$ in Figure 1 shows vibronic structure as barely resolved shoulders across the luminescence band. The luminescence spectrum of $[K(18\text{-crown-}6)]_2Pd(SCN)_4$ in Figure 2 does not show any resolved vibronic structure. In contrast, the spectrum of $(LC)_2Pd(SCN)_4$ in Figure 3 consists of clearly resolved vibronic transitions. The highest-energy maximum is at 14450 cm^{-1}, and the main progression has an average interval of 276 ± 8 cm^{-1}, corresponding to the vibrational mode observed at 278 cm^{-1} in the Raman spectrum. This vibration is assigned as the totally

(19) Mawby, A.; Pringle, G. E. *J. Chem. Soc., Chem. Commun.* **1970**, 385.
(20) Mawby, A.; Pringle, G. E. *J. Inorg. Nucl. Chem.* **1972**, *34*, 2213.
(21) Sridhar, M. A.; Indira, A.; Prasad, J. S.; Cameron, T. S. *Z. Kristallogr.* **1994**, *209*, 437.
(22) Sabatini, A.; Bertini, I. *Inorg. Chem.* **1965**, *4*, 959.
(23) Davis, M. J.; Reber, C. *Inorg. Chem.* **1995**, *34*, 4585.
(24) Rohde, J.-U.; von Malottki, B.; Preetz, W. *Z. Anorg. Allg. Chem.* **2000**, *626*, 905.

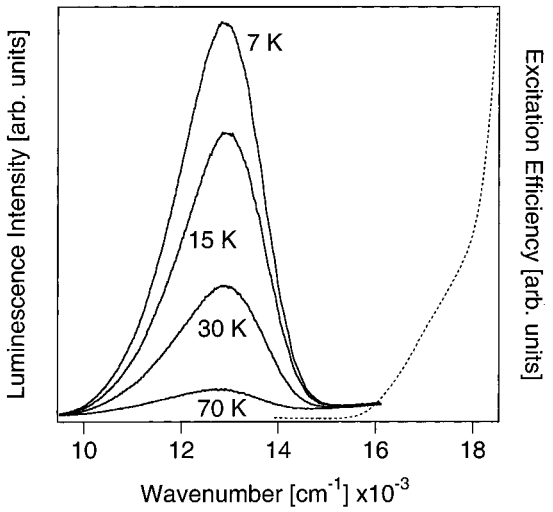

Figure 2. Luminescence and excitation spectra of $[K(18\text{-crown-}6)]_2Pd(SCN)_4$. Luminescence spectra at 7, 10, 20, and 70 K (top to bottom) are given as solid lines; the excitation spectrum at 7 K is shown as a dotted line.

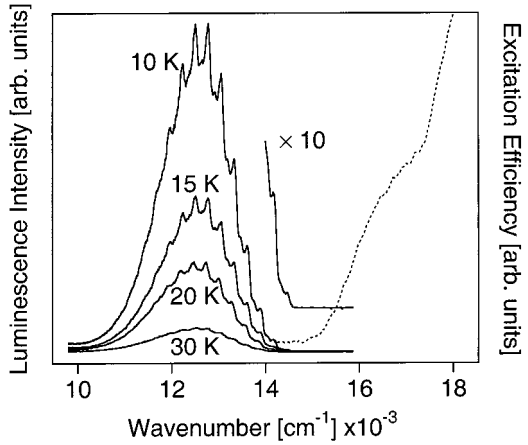

Figure 3. Solid-state excitation and luminescence spectra of (2-diethylammonium *N*-(2,6-dimethylphenyl)acetamide)$_2$Pd(SCN)$_4$. Luminescence spectra at 10, 20, and 70 K (top to bottom) are given as solid lines. The origin region of the 10 K spectrum is enlarged by a factor of 10 and offset along the ordinate for clarity. The 10 K excitation spectrum is given as a dotted line.

symmetric stretching mode by comparison with the spectra and normal coordinate analysis of the PdS_4 fragment in $(n\text{-}Bu_4N)_2Pd(SCN)_4$.[24] A second set of peaks is observed at an average energy lower by 150 ± 20 cm^{-1} than the maxima of the main progression, an energy interval in the range of the Raman transitions corresponding to modes with predominant S−Pd−S bending character,[24] denoted as b_{2g} in Table 1. All these modes involve the SCN^- ligands, and more than the single ligand−Pd−ligand bending frequency expected for the PdS_4 fragment in the idealized D_{4h} point group is observed. The asymmetric b_{1g} stretching mode is observed at 260 cm^{-1} in the Raman spectra of the title compound and in the literature study on $(n\text{-}Bu_4N)_2Pd(SCN)_4$[24] and does not correspond to distinct maxima in the resolved vibronic structure of the luminescence spectra. The ratio of the b_{1g} and a_{1g} frequencies is approximately 0.9 for the title compound, identical to that for $(n\text{-}Bu_4N)_2Pd(SCN)_4$[24] and within a few percent of the ratio of the stretching frequencies observed for $PtCl_4^{2-}$, $PdCl_4^{2-}$, and $PdBr_4^{2-}$,[25,26] further confirming the Raman assignments in Table 1.

The luminescence intensities for all crystals decrease rapidly with increasing temperature. No luminescence is observed for $K_2Pd(SCN)_4$ at temperatures higher than 30 K, an observation in agreement with a literature report of the absence of luminescence above liquid nitrogen temperature.[9] The spectra at selected temperatures included in Figures 1−3 indicate that the band maxima and widths do not show any dramatic changes in the temperature range where luminescence can be observed. The resolved vibronic structure in the spectrum of $(LC)_2Pd(SCN)_4$ is broadened, but still easily discernible at 30 K.

Luminescence lifetimes in the millisecond range are measured at low temperatures, typical for the spin- and parity-forbidden electronic transitions expected for the square-planar title compound. Experimental lifetimes determined at the luminescence band maximum at selected temperatures are included in Table 1. Luminescence decay curves were measured at five wavelengths across the emission bands. These low-temperature lifetimes vary by less than 2%, indicating that the inhomogeneously broadened luminescence spectra arise from very similar luminophores. The decrease of the lifetimes with temperature is similar to that of the luminescence intensities in Figures 1−3.

The excitation spectra of the lowest-energy electronic transition measured in a 5 nm wavelength interval at 796 nm are given in Figures 1 to 3 and the excitation maxima are summarized in Table 1. The lowest-energy band for all crystals is weak and does not show resolved vibronic structure. The onset of more intense higher-energy bands leads to the increasing excitation efficiency toward the high-energy end of the wavenumber scales in Figures 1−3. Polarized single-crystal absorption spectra[9] of $K_2Pd(SCN)_4$ show a weak, unpolarized band in the same energy range and with a band shape very similar to that of the excitation spectrum in Figure 1.

The Stokes shifts for the title complex in all three crystal environments are on the order of 4000 cm^{-1} as listed in Table 1, smaller by approximately 1000 cm^{-1} than for $K_2Pt(SCN)_4$.[9] A similar reduction of the Stokes shift by approximately 30% was previously reported for K_2PdBr_4 and K_2PdCl_4[14] in comparison to their platinum(II) analogues.[10,11]

Discussion

Resolution of the Electronic Spectra, Luminescence Lifetimes, and Intensities. The luminescence spectra in Figures 1−3 show different resolution as well as luminescence intensities and lifetimes that vary strongly with temperature. The resolution of the spectra is most likely determined by inhomogeneous broadening, and a qualitative correlation between the magnitude of the inhomogeneous broadening and the size of the cations can be established. The best resolution is obtained for the large, low-symmetry LC cation. These crystals have well-separated $Pd(SCN)_4^{2-}$ chromophores at crystallographically identical sites with inversion symmetry at the metal center.[21] The Pd−S bond lengths are 2.323 and 2.340 Å for the two perpendicular pairs of bonds, and the two inequivalent SCN^- ligands are bent out of the crystallographically exact PdS_4 plane by 0.5° and 15°, respectively.[21] The smaller of the two S−Pd−S angles is 89.3°, leading to a point group symmetry very close to D_{4h} for the PdS_4 fragment. The structure of the chromophore deviates more strongly from D_{4h} in $K_2Pd(SCN)_4$, but the palladium center still has inversion symmetry.[19,20] Perpendicular metal−ligand bond lengths are 2.312 and 2.392 Å, respectively, and the inequivalent SCN^- ligands deviate by 16.2° and 70.2° from the crystallographically exact PdS_4 plane. It is tempting to attribute the very rapid decrease of the luminescence intensity

(25) Bosworth, Y.; Clark, R. J. H. *Inorg. Chem.* **1975**, *14*, 170.
(26) Chen, Y.; Christensen, D. H.; Nielsen, O. F.; Hyldtoft, J.; Jacobsen, C. J. H. *Spectrochim. Acta* **1995**, *51A*, 595.

with temperature to the lower symmetry of the chromophore in the potassium salt, leading to relaxed symmetry restrictions on high-frequency ligand-centered accepting modes. Energy transfer processes to deep traps are also expected to be more efficient in the potassium salt, which has the closest packing of $Pd(SCN)_4^{2-}$ among the three crystalline materials investigated here. The influence of these two effects on the phenomenological relaxation behavior is qualitatively confirmed by $[K(18\text{-crown-}6)]_2Pd(SCN)_4$: the luminescence intensity decreases much slower with increasing temperature than in $K_2Pd(SCN)_4$, and the larger separation between anions leads to weak intermolecular interactions that do not cause large angles between the SCN^- axis and the PdS_4 plane.

The excitation spectra do not show resolved structure, and their band shapes are very similar to that of the absorption spectrum reported for $K_2Pd(SCN)_4$.[9] In contrast, the corresponding absorption bands of complexes with exact D_{4h} symmetry such as $PdBr_4^{2-}$ show resolved vibronic structure.[14] It is likely that this difference is a consequence of the low C_i point group symmetry of the title complex, which leads to a splitting of the ^3E_g excited state and to overlapping absorption transitions that are not resolved. Density functional MO calculations[27] for $Pd(SCN)_4^{2-}$ using the crystallographic coordinates of $(LC)_2Pd(SCN)_4$ lead to an energy difference of 180 cm^{-1} between the HOMO and HOMO-1 orbitals, which correspond to the degenerate $e_g(d_{xz},d_{yz})$ orbitals in both the idealized D_{4h} symmetry of the PdS_4 fragment and the C_{4h} idealized symmetry of $Pd(SCN)_4^{2-}$. This separation is on the same order of magnitude as the energy intervals observed in the resolved luminescence spectra. The overlapping transitions to states arising from both the $(HOMO)^1(LUMO)^1$ and the $(HOMO\text{-}1)^1(LUMO)^1$ configurations are observed in the absorption and excitation spectra, leading to spectra without resolved vibronic structure, as reported in Figures 1−3. Luminescence occurs only from the lowest-energy excited state arising from the $(HOMO)^1(LUMO)^1$ configuration, and the spectra show more resolution. The calculated separation of the HOMO and HOMO-1 orbitals is smaller by almost 2 orders of magnitude than the HOMO−LUMO energy difference of 14700 cm^{-1}. The model calculations on an isolated complex justify our use of symmetry labels for the idealized D_{4h} point group symmetry.

For some square-planar complexes, such as $PtCl_4^{2-}$ and $PdBr_4^{2-}$, a separation of up to 1800 cm^{-1} is observed between the onsets of luminescence and absorption or excitation spectra.[11,14] This energy gap is larger by at least a factor of 4 than any vibrational mode of the complexes and is due to coupling between excited states that leads to an emitting-state potential with two equally deep minima separated by a flat maximum at the ground-state equilibrium geometry.[11,13,14] Such large gaps are not observed for $Pd(SCN)_4^{2-}$ in Figures 1−3, where the onsets of luminescence and excitation spectra are separated by approximately 300 cm^{-1}, a difference most likely caused by ungerade parity enabling modes. Coupling effects between the two orbital components of the ^3E_g excited state of $Pd(SCN)_4^{2-}$, which both have A_g symmetry in the C_i point group of crystalline $Pd(SCN)_4^{2-}$,[19−21] do not lead to an energy gap between excitation and luminescence spectra. The energy difference between the low-symmetry split components of the emitting state shifts the crossing region of the potentials away from the ground-state equilibrium geometry, and no maximum of the emitting-state surface in the Franck−Condon region is obtained. Both the absence of vibronic structure in the excitation spectra and the absence of an energy gap are spectroscopic evidence for the deviation from perfect D_{4h} symmetry in the title complex. The resolved luminescence spectra involve only the lowest-energy component of the ^3E_g emitting state and allow us to define average emitting-state properties for the ensemble of luminescent species forming the inhomogeneously broadened spectra, as described in the following section.

Table 2. Parameters Used for the Calculation of Luminescence Spectra

parameter	$K_2Pd(SCN)_4$	$(LC)_2Pd(SCN)_4$	
vibrational energies (ground and emitting state)			
$k_{a_{1g}}$ (cm^{-1})	277[a]	278[a]	278[b]
$k_{b_{1g}}$ (cm^{-1})	*d*	*d*	260[b]
$k_{b_{2g}}$ (cm^{-1})	160[a]	148[a]	152[b]
$k_{b_{2g}}'$ (cm^{-1})	*d*	*d*	132[b]
E_{00} (cm^{-1})	14,450	14,450	14,450
$\Delta_{a_{1g}}$[c]	3.75[a]	3.74[a]	3.52[b]
$\Delta_{b_{1g}}$[c]	*d*	*d*	1.18[b]
$\Delta_{b_{2g}}$[c]	1.94[a]	1.61[a]	1.00[b]
$\Delta_{b_{2g}}'$[c]	*d*	*d*	1.26[b]
Γ (cm^{-1})[c]	60	40	40

[a] Two-mode model using the a_{1g} Raman frequency and an average b_{2g} frequency. [b] Four-mode model using the a_{1g}, b_{1g}, and two b_{2g} Raman frequencies. [c] From the calculated spectra in Figure 4. [d] Not applicable.

Vibronic Structure of the Luminescence Spectra and Emitting-State Properties. The vibronic structure observed for $K_2Pd(SCN)_4$ and for $(LC)_2Pd(SCN)_4$ is calculated from models involving harmonic potential energy surfaces with identical vibrational energies in the ground and emitting electronic states. Emitting-state vibrational frequencies lower by up to 20% than the ground-state values in Table 1 do not lead to a significantly different position of the emitting-state potential energy surface along the normal coordinates dominating the vibronic structure. Luminescence of the title compound occurs only from the lowest-energy component of the ^3E_g excited state, and we use a single potential energy surface to represent the emitting state.

The first model is based on the two resolved vibronic progression intervals observed in the luminescence spectra in Figure 3, assigned to the a_{1g} stretching and b_{2g} bending modes, and is denoted as the two-mode model throughout this discussion. The vibrational energies $k_{a_{1g}}$ and $k_{b_{2g}}$ in wavenumber units used to define the potential surfaces along the $Q_{a_{1g}}$ and $Q_{b_{2g}}$ normal coordinates are given in Table 2. We choose the ground-state potential minimum as the origin of the coordinate system consisting of the $Q_{a_{1g}}$ and $Q_{b_{2g}}$ axes. The only adjustable parameters are the two offsets $\Delta_{a_{1g}}$ and $\Delta_{b_{2g}}$ in dimensionless units that define the position of the emitting-state minimum along the normal coordinates. The emitting-state potential E in wavenumber units is given by

$$E = \frac{1}{2}(k_{a_{1g}}(Q_{a_{1g}} - \Delta_{a_{1g}})^2 + k_{b_{1g}}(Q_{b_{2g}} - \Delta_{b_{2g}})^2) + E_{00} \quad (1)$$

E_{00} denotes the energy offset between the minima of the ground- and emitting-state potential surfaces in wavenumber units. The maximum of the highest-energy observed luminescence peak in Table 1 was used for all calculations.

(27) SPARTAN 5.1, Wavefunction, Inc., 18401 Von Karman Ave., Suite 370, Irvine, CA 92612. The density functional method, SVWN model, and DN basis set were used.

(28) Heller, E. J. *J. Chem. Phys.* **1975**, *62*, 1544−1555.
(29) Heller, E. J. *Acc. Chem. Res.* **1981**, *14*, 368.
(30) Zink, J. I.; Kim Shin, K.-S. In *Advances in Photochemistry*; Volman, D. H., Hammond, G. S., Neckers, D. C., Eds.; John Wiley: New York, 1991; Vol. 16; p 119.

We use time-dependent theory to calculate the luminescence spectra. The luminescence intensity is given by[28−30]

$$I_{lum}(\omega) = C\omega^3 \int_{-\infty}^{+\infty} e^{i\omega t}\{\langle\phi|\phi(t)\rangle e^{-\Gamma^2 t^2 + (iE_{00}/\hbar)t}\}\, dt \quad (2)$$

ω denotes the wavenumber value for which the luminescence intensity I_{lum} is calculated, C is a constant to scale the relative intensity, and Γ is a phenomenological damping factor in wavenumber units defining the width of each line in the luminescence spectrum. This width is determined by inhomogeneous broadening. The autocorrelation function $\langle\phi|\phi(t)\rangle$ is the most important ingredient to calculate the luminescence spectrum with eq 2. It is a product of the individual autocorrelation functions along each normal coordinate k (k: a_{1g}, b_{2g}):[25−27]

$$\langle\phi|\phi(t)\rangle = \prod_k \langle\phi_k|\phi_k(t)\rangle \quad (3)$$

The autocorrelation function for one-dimensional harmonic potentials along a normal coordinate k (k: a_{1g} or b_{2g}) with identical vibrational energies is given in the literature in analytical form as[29,30]

$$\langle\phi_k|\phi_k(t)\rangle = \exp\left[-\frac{\Delta_k^2}{2}(1 - \exp(-i\omega_k t)) - \frac{i\omega_k t}{2}\right] \quad (4)$$

The luminescence spectra calculated with the two-mode model are compared to the experimental data in Figure 4 for $K_2Pd(SCN)_4$ and $(LC)_2Pd(SCN)_4$, and the values of all model parameters are given in Table 2. The overall agreement between experimental spectra and the calculations using the two-mode model is good, especially since only the two Δ_k values were treated as adjustable parameters. The vibrational frequencies and luminescence band envelopes are similar for both compounds, leading to values for $\Delta_{a_{1g}}$ that are identical to within our precision and similar to the values of 3.7 and 3.9 obtained from the luminescence spectra of $PdCl_4^{2-}$ and $PdBr_4^{2-}$, respectively.[14] The $\Delta_{b_{2g}}$ values determined with the two-mode model for $K_2Pd(SCN)_4$ and $(LC)_2Pd(SCN)_4$ in Table 2 differ by less than 15%. The Δ_k values for the latter compound correspond to Huang−Rhys parameters $S_{a_{1g}}$ and $S_{b_{2g}}$ of 7.0 and 1.3, respectively, leading to a ratio $S_{a_{1g}}/S_{b_{2g}}$ of 5.4. This value is smaller by more than a factor of 3 than the lower limit for $S_{a_{1g}}/S_{b_{2g}} > 18$ derived from the electrostatic ligand-field potential in a recent theoretical study,[31] underlining the importance of experimental electronic spectra for the determination of excited-state distortions.

The temperature dependence of the luminescence spectrum of $(LC)_2Pd(SCN)_4$ can be reproduced by increasing the phenomenological damping factor Γ, as illustrated in Figure 4b. A value of 50 cm^{-1} is used to reproduce the spectrum observed at 30 K and illustrates the similarity to the less-resolved experimental spectrum of $K_2Pd(SCN)_4$ in Figure 4a. Calculated spectra at higher resolution than the best fit are included in Figure 4a and illustrate the detailed vibronic pattern arising from the two-mode model.

An improvement of the two-mode model has to address two key discrepancies between the calculated spectrum shown as a dotted line in Figure 4b and the spectroscopic data. First, the b_{2g} frequency used in the two-mode model for $(LC)_2Pd(SCN)_4$ is within the energy interval determined from the luminescence spectrum, but does not correspond exactly to a vibrational energy observed in the Raman spectrum. We therefore include the *two*

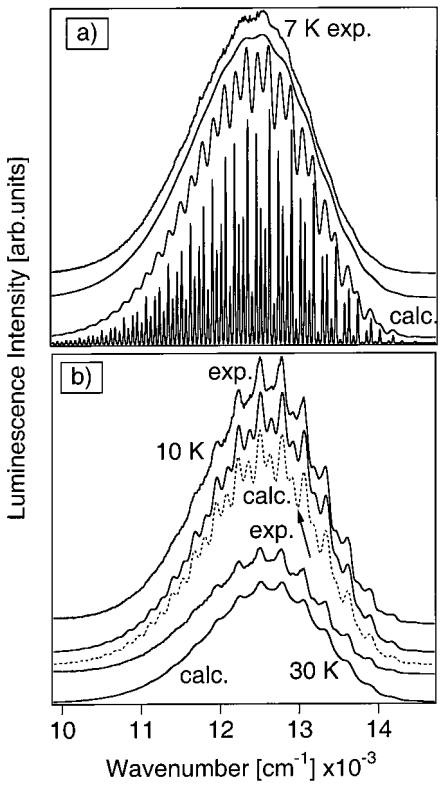

Figure 4. Calculated and experimental luminescence spectra of $Pd(SCN)_4^{2-}$. Traces are offset along the ordinate for clarity. (a) $K_2Pd(SCN)_4$. Top to bottom: experimental spectrum at 7 K; best-fit calculated spectrum with the parameters for the two-mode model in Table 2; intermediate-resolution calculated spectrum with the parameters in Table 2, except $\Gamma = 30$ cm^{-1}; high-resolution calculated spectrum with the parameters in Table 2, except $\Gamma = 5$ cm^{-1}. (b) $(LC)_2Pd(SCN)_4$. Top to bottom: experimental spectrum at 10 K; best-fit calculated spectrum with the parameters for the four-mode model in Table 2; (dotted line) best-fit calculated spectrum for the two-mode model in Table 2; experimental spectrum at 30 K; calculated spectrum with the parameters in Table 2, except $\Gamma = 50$ cm^{-1}.

most intense vibrational frequencies in the S−Pd−S stretching region to define the improved model. Second, the agreement between the experimental and calculated luminescence spectra is not very good in the region close to the maxima of the main progression, where the calculated spectrum shown as a dotted line in Figure 4b has minima that are much lower than observed in the experiment. The arrow in Figure 4b denotes one of these deep minima. The difference is most pronounced around the band maximum and to the low-energy side of the spectrum, indicating the presence of unresolved vibronic features involving a mode with a frequency close to that of the a_{1g} stretching mode. The b_{1g} stretching mode, of importance in the luminescence spectra of square-planar halide complexes of platinum(II) and palladium(II), is closest in frequency, and we have included it to calculate the emitting-state potential surface with nonzero offsets Δ_k along four normal coordinates. The autocorrelation for each mode is calculated with eq 4 where k denotes a_{1g}, b_{1g}, b_{2g}, and b_{2g}'. The spectrum calculated with this four-mode model is shown as a solid trace below the experimental spectrum measured at 10 K in Figure 4b, and the parameters used are given in the rightmost column of Table 2. The agreement with the experiment is improved, and we note that the distortions for the a_{1g} and b_{2g} modes are close to those obtained from the two-mode model, an important control because the vibronic transitions involving the energetically close pairs of modes are not individually resolved. The distortion along the b_{1g} stretching

(31) Wissing, K.; Degen, J. *J. Mol. Struct.* **1998**, *431*, 97.

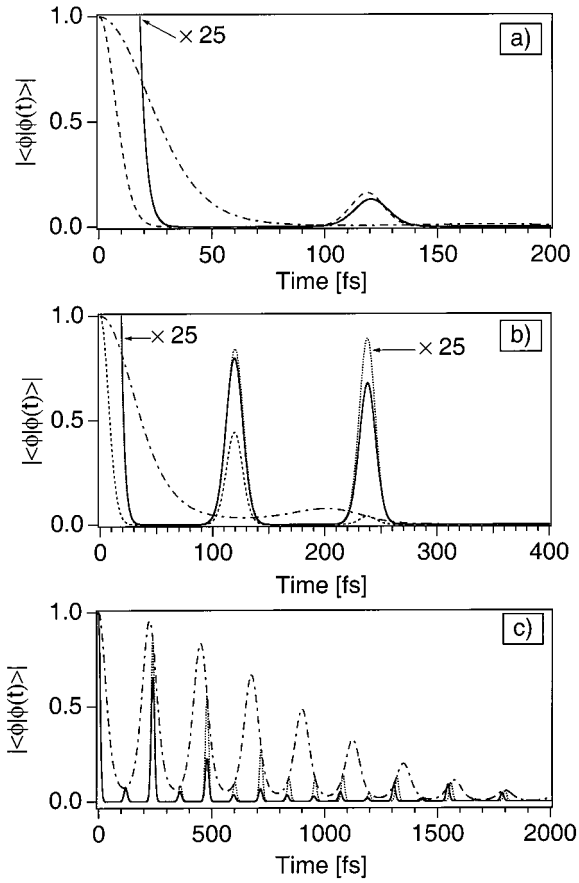

Figure 5. Absolute autocorrelation functions calculated with different damping factors Γ. (a) $K_2Pd(SCN)_4$. Solid line: absolute autocorrelation used for the calculation of the best-fit spectrum in Figure 4a enlarged by a factor of 25 with respect to the ordinate scale given (Γ = 60 cm^{-1}). Dotted line: autocorrelation for the 277 cm^{-1} mode. Dash−dotted line: autocorrelation for the 166 cm^{-1} mode. (b) $(LC)_2Pd(SCN)_4$ (Γ = 40 cm^{-1}). Solid line: total autocorrelation for the four-mode model used to calculate the spectrum shown as a solid line in Figure 4b. Dotted line: total autocorrelation for the two-mode model leading to the spectrum shown as a dotted line in Figure 4b. Dash−dotted lines: absolute autocorrelation functions of the a_{1g} and b_{2g} modes of the two-mode model. (c) $(LC)_2Pd(SCN)_4$ (Γ = 1 cm^{-1}). Solid line: absolute autocorrelation function for the four-mode model. Dotted line: absolute autocorrelation function for the two-mode model. Dash−dotted line: absolute autocorrelation function of the 132 cm^{-1} b_{2g} mode used in the four-mode model.

coordinate is significantly smaller than the total distortions along the b_{2g} bending modes, a situation not reported for a square-planar metal complex before. The four-mode model leads to a ratio $S_{a_{1g}}/S_{b_{1g}}$ of 8.9, again smaller by approximately a factor of 3 than the lower limit of $S_{a_{1g}}/S_{b_{1g}} \geq 25$ given in the literature.[31]

The relationship between the two-mode model and the four-mode model is quantitatively illustrated by the comparison of the absolute autocorrelation functions in Figure 5. Figure 5a shows the absolute autocorrelation functions calculated for $K_2Pd(SCN)_4$ with a damping factor Γ of 60 cm^{-1}. The product function calculated with eq 3 is shown as a solid line. Only a single recurrence at 121 fs appears in the solid trace. This time is significantly longer than for the 277 cm^{-1} mode alone (dotted line), where a recurrence occurs at 119 fs. The longer recurrence time for the product autocorrelation is caused by the 160 cm^{-1} mode whose first recurrence is outside the time range of Figure 5a. The product recurrence time of 121 fs leads to the vibronic spacing of 276 cm^{-1} in the best-fit calculated spectrum shown in Figure 4a. This spacing does not correspond exactly to a

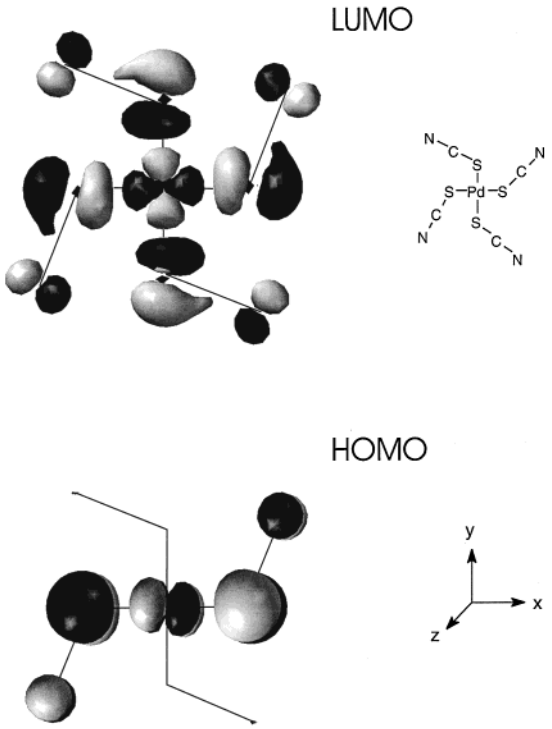

Figure 6. HOMO and LUMO orbitals of $Pd(SCN)_4^{2-}$ obtained from density functional calculations. The schematic structure of the title complex and the Cartesian axis system used are included.

ground-state vibrational mode, and the apparent separation between maxima of the calculated spectrum is a MIME.[17] A similar effect involving the a_{1g} and b_{1g} stretching modes was analyzed in detail for K_2PtCl_4.[11]

Figure 5b shows the absolute autocorrelation functions used to calculate the spectra for $(LC)_2Pd(SCN)_4$ shown at 10 K in Figure 4b on a time scale twice as long as in Figure 5a. Again, the recurrence times of the product autocorrelations for both the two-mode and four-mode models are different from those of the 278 cm^{-1} mode, but since the damping factor Γ is smaller than in Figure 5a several recurrences determine the calculated vibronic structure in Figure 4b, leading to resolved maxima for both modes in the two-mode model and for MIME phenomena only within the two pairs of energetically close modes in the four-mode model. The autocorrelation functions of the two- and four-mode models in Figure 5b have their first recurrences at times that vary by only 0.4 fs, a small difference that leads to the very similar vibronic maxima of the spectra calculated with these two models and compared in Figure 4b.

Figure 5c shows the autocorrelation functions of the two- and four-mode models for $(LC)_2Pd(SCN)_4$ on a time scale longer by a factor of 5 than in Figure 5a. This time scale is necessary to calculate highly resolved spectra, such as the bottom trace of Figure 4a. The dash−dotted line is the autocorrelation calculated with eq 4 for the lowest-frequency mode in the four-mode model. The modulation of the product autocorrelation functions from eq 3 by this "slowest" mode is obvious. At times longer than 1000 fs the recurrences for the two- and four-mode models no longer coincide, clearly illustrating the differences between the two models in the time domain.

The analysis of the luminescence spectra with time-dependent theory indicates that the emitting-state properties of the title complex in all three crystal environments are very similar, despite the varying resolution of the spectra in Figures 1−3. The luminescence spectra show distinct vibronic structure involving mainly the a_{1g} stretching and the b_{2g} bending

vibrational modes, allowing us to quantitatively characterize the effects arising from population changes of σ and π antibonding orbitals on the potential energy surfaces of the ground and emitting states.

The origin of the unusual distortion along S−Pd−S bending coordinates is qualitatively illustrated by the shapes of the HOMO and LUMO molecular orbitals obtained from density functional calculations[27] and shown in Figure 6. The HOMO orbital has significant d_{xz} character, but the wave function amplitude is not symmetrically distributed above and below the Pd−S bonds that coincide with the *x* axis. The d electron density is directed toward the lone pair region of the sulfur atoms. In contrast, the wave function amplitude of the LUMO orbital is almost symmetric around each Pd−S bond, and the electron density is even slightly tilted away from the lone-pair region of the sulfur atoms. These differences produce a large change in angular wave function amplitude distribution during a HOMO ↔ LUMO excitation and lead to the observed vibronic structure involving S−Pd−S bending modes. Such a change of the radial electron density does not occur in the halide complexes, where the distortion along the b_{1g} stretching coordinate dominates any effect along a bending coordinate, as illustrated by the calculated potential energy surfaces and luminescence spectra of $PdCl_4^{2-}$ and $PdBr_4^{2-}$.[14,18] This comparison shows that simple monodentate ligands are sufficient to control the type and magnitude of the distortions occurring in the long-lived emitting state of square-planar palladium(II) complexes.

Acknowledgment. We thank Hugo Bélisle (Université de Montréal) for measuring the Raman spectra and Jesper Bendix (Universität Bern) for helpful discussions. This work was made possible by grants from the Natural Sciences and Engineering Research Council (Canada).

IC000133L